Carbon 199 (2022) 141–150

Contents lists available at ScienceDirect

Carbon

journal homepage: www.elsevier.com/locate/carbon

Post-plasma oxidation in water of graphene paper surface

Paweł Stelmachowski *, Karolina Kadela, Gabriela Grzybek, Monika Gołda-Cępa, Krzysztof Kruczała, Andrzej Kotarba

Jagiellonian University, Faculty of Chemistry, Gronostajowa 2, 30-387, Krakow, Poland

A B S T R A C T

Plasma activation is increasingly used to tailor the electronic properties of carbon materials by surface functionalization, especially with various oxygen groups. However, the actual application of these materials may be some time after the modification was performed, and what is more, in a different environment, e.g. in an aqueous solution. The presented research addresses the problem of instability of plasma-induced changes of graphene paper material where the desired surface property – work function – was verified just after plasma treatment and after bringing the plasma-treated surface to a stable state. In this study, we optimised plasma treatment for the maximum work function changes, and then we determined the speciation of the resulting oxygen groups before and after immersion of the plasma-treated samples in water. We found that the plasma-modified graphene paper's functionalization degree and electronic properties highly depend on the post-plasmatic reactions in water, which increase the concentration of surface oxygen groups. The observed reactivity is rationalized in terms of plasma-emitted irradiation in the ultraviolet range resulting in an enhanced delocalized radical species generation. These radicals react upon contact with water and increase the number of oxygen functional groups.

1. Introduction

Surface reactivity modification of carbons, especially of graphene and graphene-related materials, is of continuously increasing interest to the scientific community. Work function (WF, Φ) is a surface-sensitive parameter describing the electron-donor properties of the materials. It is a key parameter of materials especially in heterogeneous catalysis [1–4], in electrochemistry [5,6], and biocompatible medical elements [7–9]. Work function of a material is defined as the minimum energy required for moving an electron from the Fermi level into the vacuum. Its value gives information about the electronic properties of the solid surface. It is a key parameter in describing charge exchange events at interfaces. Work function has been widely studied for model metal surfaces promoted with alkali [10]. The promotional effect of alkali is mainly related to their low ionization potentials which allow for a charge transfer to the material surface, inducing an electric field gradient at the surface, generated by the resulting dipole moment. This is especially pronounced in the case of heavier alkali atoms due to their large ionic radii which in turn gives rise to large values of the dipole moment and the associated work function changes. The introduction of oxygen functionalities onto a carbon surface changes it from super-hydrophobic to a completely wettable one, modifies its acid-base properties, and enhances the adsorption by formation of new active centers. The electronic effect, however, is opposite to alkali addition, since the partial negative charge is located at the surface, and negative charge just below the surface, which leads to an increase of the material's work function [7]. Although the work function can be calculated from the first principles [11], it is not trivial, and sometimes only changes in the electrostatic potential are determined [12]. Since the work function is one of the most sensitive parameters characterizing surface electronic properties, it can be succesfully used to monitor the changes of oxygen functional groups coverage in carbon materials.

Work function tuning of graphene materials surfaces is of particular interest due to the application of graphene as both anode and cathode in organic field-effective transistors, organic light-emitting diodes, and organic photovoltaic cells. Apart from the other required characteristics of the electrode material, the interface between the semiconductor and electrodes has to be optimised to maximize the performance of the device. As recently reviewed in Ref. [5] any incompatibility of the work functions of organic semiconductors and electrodes will result in high contact resistance, which will lead to a decrease in the charge injection and extraction efficiency. It was pointed out that a design of graphene with both high electron injection (low WF) and high hole injection (high WF) abilities is in demand. Therefore, extensive research effort has been exerted in the last decade to develop modulation methods for tuning the WF of graphene. Following this strategy, a technique of controllable wettability modification through low-damage plasma O_2/H_2 treatment of graphene to introduce oxygen functional groups (OFG) was evaluated

* Corresponding author.
E-mail address: pawel.stelmachowski@uj.edu.pl (P. Stelmachowski).

https://doi.org/10.1016/j.carbon.2022.07.031
Received 30 May 2022; Received in revised form 11 July 2022; Accepted 12 July 2022
Available online 30 July 2022

for potential application in graphene-based sensors/devices [13]. Similarly, nitrogen plasma under different conditions was shown to be able to decrease the work function of graphene by 0.54 eV to optimize the efficiency of optoelectronic and electronic devices [14].

Plasma surface modification techniques are also used in the context of carbon biomaterials, where surface electron-donor properties determine the successful performance of the medical device in the body. One of the strategies to prevent the attachment of pathogenic bacteria possessing a net negative charge to the biomaterials is to lower their work function [8,15]. It was found, that the concentration of surface oxygen groups is a key factor in bacterial adhesion to graphenic surfaces [9].

Electrocatalytic materials, especially for the oxygen reduction reaction (ORR), reveal a correlation between their work function and ORR reactivity. It was concluded that the work function of the heteroatom doped nanocarbons and other carbon-based formulations can be generally used as an activity descriptor for the ORR and can be applied as a design principle for the development of advanced electrocatalysts for other important reactions [6,16]. Moreover, the work function tailoring via graphene shell encapsulation of transition metals was shown to be a powerful approach for the preparation of highly durable non-precious metal nanostructures for ORR [17].

Surface modification with different functional group types, even of the same element – oxygen, leads to different WF changes. The functionalization with oxygen groups can be effectuated by various methods, such as thermal treatment, wet acid treatment, electrochemical oxidation, or plasma oxidation. It was shown that the oxidation of multiwall carbon nanotubes (MWCNT) by heating in air flow mainly introduces hydroxyl and carbonyl groups and results in a moderate increase of the work function. On the other hand, plasma treatment destroys the π-conjugation, forms an amorphous carbon phase, and introduces surface dipole moments, while substantially increasing the work function. Wet acid-oxidation introduces the highest fraction of carboxylic acid groups on the surfaces of MWCNTs and produces the highest work function material [18]. Although acid treatment of carbon materials is usually associated with the introduction of the highest number of carboxylic groups, a high level of carboxylic groups can be also added to the carbon nanotubes as a result of the plasma treatment [19]. The final work function change depends on the degree of the plasma modification. In Ref. [12] two different modification effects of MWCNTs were identified and associated with various oxygen adatom locations: out-of-plane (C_{surf}-O_{adatom}) and in-plane (C_{surf}-O_{surf}-C_{surf}). It was found that the formation of surface oxygen groups promotes the work function increase by creating isolated dipoles, whereas deeper subsurface and bulk oxidation leads to a reversed effect – work function decrease. It was concluded that the work function is a suitable descriptor of the degree of functionalization restricted to the surface and an indicator of subsequent MWCNT amorphization. Recently, it was calculated that different oxygen functional groups, such as C–OH, C═O, and –COOH, result in different WF changes for the same number of surface O atoms. In particular, the introduction of HO–C═O groups results in the lowest WF increase, while for C–O–C groups the increase is the highest. The C═O and C–OH groups were shown to influence WF changes similarly, with the magnitude between the two former groups [20]. It was also shown that the number and type of surface oxygen groups have a great influence on ORR activity [21].

Oxidative plasma treatment leads to surface functionalization of carbon surfaces due to the formation of reactive plasma species – ions, radicals, electrons – which react with the surface of the material. The surface can be activated due to the interaction with the plasma components and plasma-generated irradiation [22]. The surface modification in plasma is influenced by every parameter used to generate plasma, such as generator power, total pressure, and modification time [7,23,24]. The resulting plasma-treated surfaces are not stable in time, and it was postulated that plasma-induced changes evolve when plasma-generated surface functional groups reorient themselves to lower the surface energy as oxygen species diffuse on the surface, or recombine into H_2O, and subsequently desorb [7,25]. Moreover, it was suggested that the density of polar groups decreased non-linearly over time before reaching saturation for 7 days after treatment [23]. Significantly, in a recent study of functionalization with plasma of carbon surfaces, it was shown that regardless of the gas used the physical and chemical plasma-related effects resulted in the creation of activated surfaces. However, the induced surface changes such as increased surface roughness, increased water contact angle, and other modifications of physicochemical properties were unstable in time. The degree of surface activation decreased as the elapsed time after the modification increased [24].

Table 1
A summary of plasma conditions applied in the experiments.

	Factor	Levels	
		Min value (−1)	Max value (+1)
I	time	6 s	15 min
II	power	40 W	100 W
III	pressure	0.2 mbar	0.8 mbar

The possibility to tune the work function of graphenic surfaces and the challenges resulting from the instability of the plasma-treated surfaces motivated us to investigate the effect of water on the plasma-treated graphene paper. We aimed at optimization of plasma treatment towards maximization of the stable work function modification of graphene paper. To this end, we used five different plasma gases to evaluate the extent of possible WF changes. To allow better comparison with the literature data we also performed surface free energy calculations for pure oxygen plasma. Following the initial design of the experiments (DoE) study, we performed fine-tuning of the relevant parameter for each plasma gas. To obtain stable surface modifications, we used immersion in water to remove the electrostatic charging of the sample and promote surface reactions with H_2O. We found that after initial post-plasma reactions in the air, which occur upon sample exposure to the ambient atmosphere, the surface of graphene paper is still reactive and the concentration of oxygen functional groups still increases after immersion in water. The effect of water immersion on plasma-treated carbonaceous material is presented here for the first time.

2. Experimental

The paper graphene (GP) sheets were from Graphene Laboratories, Calverton NY, USA. The thickness of the used material was 25 μm, the density of 2 g cm^{-3}, and the conductivity $3.19 \cdot 10^5$ S m^{-1}. The samples of GP sheets were cut in the form of square pieces (usually 1 cm × 1 cm). The plasma treatment was carried out with the commercial cold plasma system using different gases: oxygen (Air Products, 99.9998% O_2), 5% O_2/He (Air Liquide, 5.000% O_2), air (Air Products, X40S COM, 2.2), Ar (Siad, 99.9998%), CO_2 (Air Products, X50S 37.5 K, ultra pure). Deionized (DI) water was obtained with HLP Hydrolab with a conductivity of 0.05 μS.

2.1. Plasma treatment

The graphene paper was modified by plasma treatment using a commercial cold plasma system (Femto - Diener Electronic GmbH, Nagold, Germany) with a generator frequency of 40 kHz. Additional details and a scheme of the device can be found in the supplementary information (SI, Fig. S 1). Pure oxygen, air, 5% O_2 in He, CO_2, and Ar were used as feed gasses for plasma generation. Optimization of plasma modification parameters was done using a design of experiments approach, where the factors were changed following Table S 1 and Table 1. The design of experiments approach was based on a 2^n factorial plan, where n is a number of factors to be investigated such as time, pressure, and power, and 2 relates to two values, the minimum and the

maximum, used to perform experiments. A series of 8 experiments were performed for each plasma gas. Table S 1 presents the parameters matrix used in the study. The exact plasma parameters applied in the experiments are presented in Table 1, where the minimum and maximum values are defined as −1 and +1, respectively. For each of the applied plasmas, an optimization of plasma modification was based on the studies of the graphene paper electronic properties – work function. As a response variable, the work function changes were used and the measurements were performed successively for the unmodified graphene paper, just after plasma treatment, and after water immersion and drying at 60 °C for several minutes. Contact angle measurements were also performed for the oxygen plasma DoE study, and surface free energy was used as a response variable.

For each type of plasma, the emission spectra measurements were performed using the spectrometer (StellarNet) and software (SpectraWiz v5.33). The parameters applied were 0.2 mbar or 0.8 mbar and for each pressure, the power was set to 20 W, 40 W, 60 W, 80 W, and 100 W. The readings were taken through the quartz window of the plasma chamber.

2.2. Work function measurements

To determine the work function changes of graphene paper the contact potential difference (V_{CPD}) was measured. Experiments were performed by the dynamic condenser method of Kelvin using a KP6500 probe (McAllister Technical Services). The stainless-steel plate was used as an electrode ($\Phi_{ref} = 4.3$ eV) with 3 mm in diameter. The measurement parameters were: the vibration frequency at 114 Hz and the amplitude at 40 a.u. To obtain a single value of V_{CPD} was measured for five backing potentials, each was an average of 32 independent measurements. 30 average points were used to obtain the final V_{CPD} value. The work function values were calculated based on the equal: $eV_{CPD} = \Phi_{ref} - \Phi_{sample}$. The work function change ($\Delta\varphi$) is equal to the difference between φ of the plasma-treated paper graphene sample (sample 2) and the reference untreated material (sample 1). It is equal to $-e$ ($V_{CPD\ (sample\ 2)} - V_{CPD\ (sample\ 1)}$). The measurements were carried out at ambient conditions (room temperature, atmospheric pressure). In situ work function measurements during ultraviolet (UV) irradiation with a 260 nm light were performed on a Kelvin probe with an Au grid as a reference electrode (Instytut Fotonowy, $eV_{CPD} = \Phi_{sample} - \Phi_{ref}$). The light source was a 150 W Xe-lamp equipped with an automatically controlled monochromator. The V_{cpd} of the reference of paper graphene was measured for 6 min in the first part, then the UV light was turned on and the sample was irradiated for 10 min, after this time the UV light was turned off.

2.3. Water contact angle measurements

The wettability and surface free energy (SFE) of paper graphene sheets were followed by the contact angle measurements with H_2O and CH_2I_2. It was carried out using a goniometer (Surftens Universal Instrument, OEG GmbH, Frankfurt (Oder), Germany). Static contact angles for at least eight 1.0 μL drops of deionized water and diiodomethane for each sample were measured using windows image processing software (Surftens 4.3). The contact angle value was an average measurement for each liquid. The SFE was calculated using the Owens-Wendt method.

2.4. Spectroscopic characterization

The X-ray photoelectron spectra were collected with a SESR4000 analyzer (Gammadata Scienta) in a vacuum chamber with a base pressure below $5 \bullet 10^{-9}$ mbar. Monochromatized Al-Kα source with the 250 W at 1486.6 eV emission energy. The pass energy for selected narrow range binding energy scans was 100 eV. CasaXPS Version 2.3.24PR1.0 was used to process the raw data [26]. The analysis of the C 1s peak was performed based on the recommended fitting procedure and spectral components [27,28]. Briefly, the main peak around 284.5 eV was modelled with three components: surface defects component (~284 eV), main graphitic carbon asymmetric peak (~284.4 eV), and disordered carbon component (~285.3 eV). HOMO-LUMO transition for primary C–C peak, π-π*, with a relatively large full width at half maximum (FWHM) is added above 290 eV. The oxygen functional groups are modelled by three components 1) C–O - ether and hydroxyl bonded C, C associated with ether bond in lactone/esters at 285.9–286.6 eV, 2) C═O - carbonyl groups and carbons attached to two ether/hydroxyl groups at 286.7–287.5 eV, and 3) COO - carboxyl, lactone and ester groups at 288.3–288.9 eV. For the plasma-treated samples, additional components at the lowest and highest binding energies were sometimes added to improve fitting quality. The fitting procedure was based on the comparison of the relative content of spectral components due to carbon-oxygen groups from the C 1s range along with the elemental composition based on C 1 s and O 1s regions. The simplest model was used to calculate the relative content of spectral components due to carbon-oxygen groups from C 1s, where the C–O and C═O peaks scale 1:1 with surface oxygen, and the COO peak is multiplied 2x. To obtain the agreement between relative oxygen content based on C 1s components and C 1s and O 1 s regions, the asymmetry of the main C–C peak was adjusted manually. The rest of the peak parameters, such as peak position, area, and FWHM resulted from the software peak fitting procedure.

The μRaman spectra of the reference and plasma-treated graphene paper samples were collected by a Renishaw InVia spectrometer equipped with a 514 nm laser. The measurements were performed in the spectral range of 1000–3000 cm^{-1} with a resolution of 1 cm^{-1}. Accumulation of ten scans was applied for each spectrum.

EPR measurements were performed at room temperature using a Bruker Elexsys E500 spectrometer operating in X-band (9.8 GHz) and 100 kHz magnetic field modulation equipped with super high sensitivity cavity ER 4122 SHQE. The spectra were recorded at 2 mW microwave power, 0.1 mT modulation amplitude, time constant 40.96 ms, and conversion time 81.92 ms. In standard experiments 4 scans were acquired. Samples were irradiated with an ER 203 UV irradiation system (50 W high-pressure mercury lamp, full light).

2.5. Experimental procedure

The reference sample was characterized with the use of XPS, Raman spectroscopy, and work function measurements. A scheme of the experimental procedure of plasma modification is presented in Fig. S 2. Before the modifications, the V_{CPD} values of the samples were measured as a reference value. Afterwards, the samples were subjected to plasma treatment, according to Table S 1 and Table 1. The graphene paper after the plasma is exposed to the ambient atmosphere, and primary post-plasma reactions occur. In addition, other surface and bulk processes take place which influence the electronic properties of the materials. Therefore, we took the initial values of the measured V_{CPD} for further analysis – taken as soon as possible after plasma treatment $V_{CPD(asap)}$. Subsequently, the same samples were immersed in water for surface stabilization and dried at 60 °C. We found that the duration of water treatment or sonication does not influence surface changes. All the water-treated samples were again measured for their V_{CPD} values, denoted as $V_{CPD(H2O)}$.

The samples with the optimised work function modifications were transferred as soon as possible after plasma treatment to the XPS vacuum chamber for spectroscopic analysis. Analogous water-treated samples were also investigated with the use of XPS. All the water-treated samples from the final optimization (usually time optimization for fixed generator power and total pressure) were investigated with Raman spectroscopy.

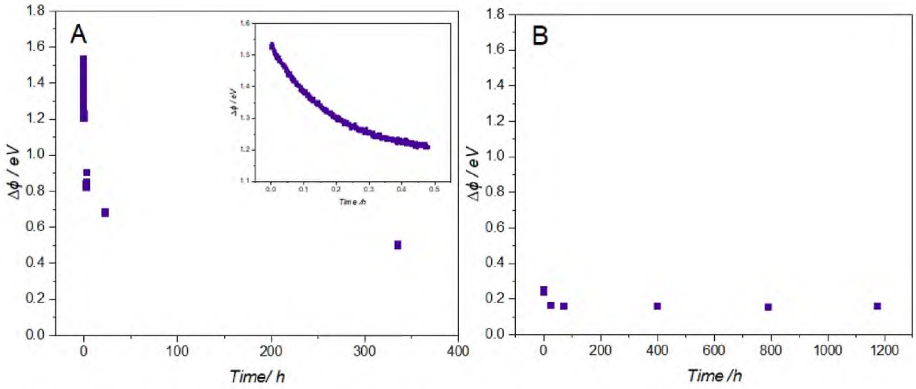

Fig. 1. Work function (contact potential difference) changes of graphene paper in time after oxygen plasma treatment (100% O_2, 100 W, 0.2 mbar, 10 min) without (A) and with water immersion (B). Inset – initial changes. (A colour version of this figure can be viewed online).

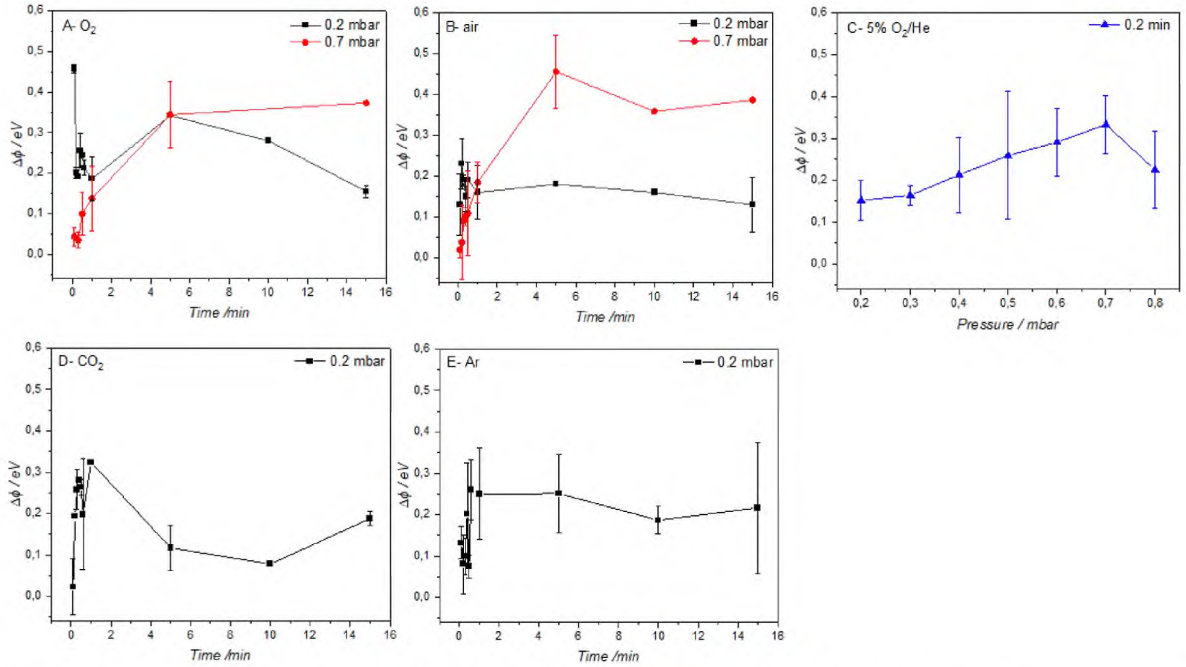

Fig. 2. Optimization of key parameters of plasma treatments based on DoE results from Fig. S 3; work function changes after immersion in water vs time for plasmas A) 100% O_2, B) air; D) CO_2, E) Ar, and pressure for plasma C) 5% O_2. (A colour version of this figure can be viewed online).

3. Results

Plasma treatment of graphene paper results in a drastic initial increase of the work function, as shown in Fig. 1A. The observed apparent work function increase diminishes quickly over time, with at least two time constants. Even after two weeks (336 h) after plasma treatment, the $\Delta\Phi$ values still change to some degree. Immersion in DI water, on the other hand, results in stable values of $\Delta\Phi$, as presented in Fig. 1B.

Statistical Design of experiments (DoE) was used to identify the parameters of used plasma treatments influencing the resulting properties of the surface to the highest extent. Design of experiments methodology is a statistical tool used for planning and conducting experiments but also analysing and interpreting data obtained from the experiments. It is a branch of applied statistics that is used to research a system, process, or product in which the input variables have been manipulated to investigate their effect on the measured response variable. This method is particularly popular in scientific areas of medicine, physics, engineering, biochemistry, and chemistry [29–31]. The DoE analysis results are presented in Fig. S 3, where the magnitude of the standardized effect of each investigated parameter is presented (parameters I, II, and III from Table S 1 and Table 1). In addition, the standardized effect of the combinations of each pair of parameters and all of them combined are also shown. Because the absolute values of $V_{CPD(asap)}$ are much higher than $V_{CPD(H2O)}$ the magnitude of the standardized effect is also higher for results taken as soon as possible after plasma treatment. From the qualitative point of view, the key factor responsible for maximal modification of the work function does not change for most samples. For the plasma parameters, where the time was most influential on the modification of electronic properties it remained so after immersion in water for 100% O_2, air, and CO_2. The total pressure in the plasma chamber influences the most WF modifications in 5% O_2/He and Ar plasma.

The optimization series of the selected critical parameter for each plasma type are presented in Fig. 2. Moreover, since for the 100% O_2 and air plasmas the combined effect of pressure and time is relatively high, the time optimization was performed for the two limiting pressure values. For the total pressure of 0.2 mbar in the plasma chamber, the electronic properties are modified to the highest extent – work function increase - in the short time range, up to about 1 min, followed by a decrease of the work function. The higher total pressure of 0.7 mbar

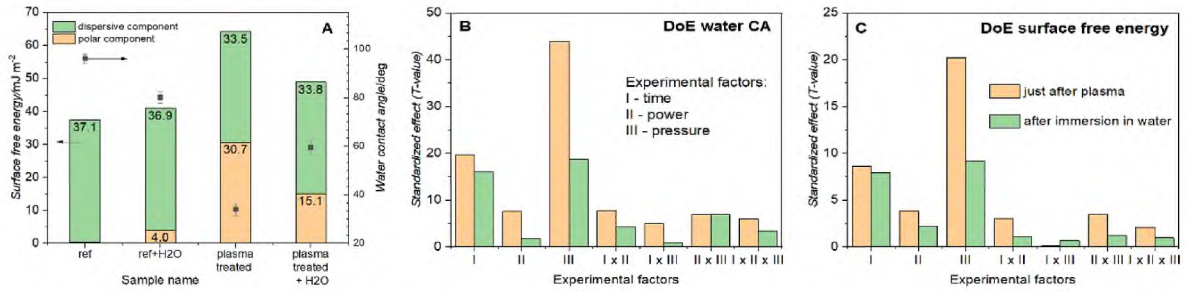

Fig. 3. Water contact angle values and Surface Free Energy calculations for the reference sample and plasma-treated (100% O_2, 100 W, 0.2 mbar, 6s) before and after immersion in H_2O accompanied by the results of the DoE. (A colour version of this figure can be viewed online).

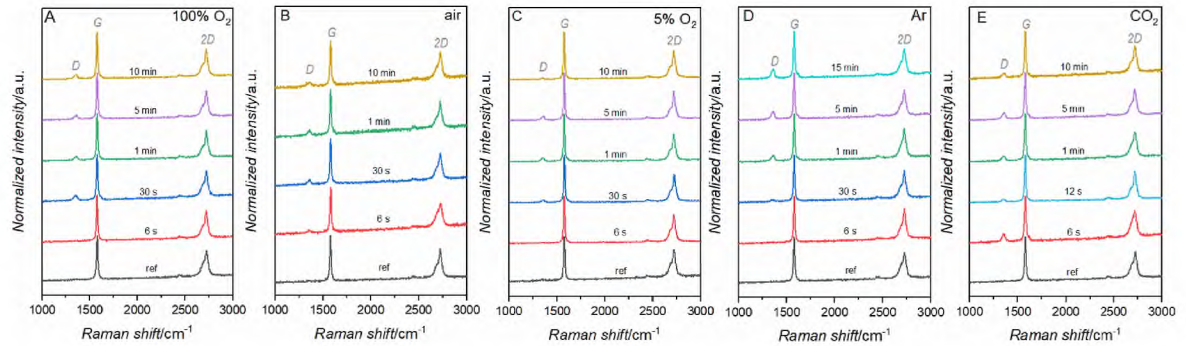

Fig. 4. Raman spectra of reference and plasma-treated graphene paper samples. Time series are used for 0.2 mbar total pressure for gases A) 100% O_2, B) air; C) 5% O_2; D) Ar, and E) CO_2. (A colour version of this figure can be viewed online).

results in more controlled modifications, with a maximum of the WF increase around after 5 min of plasma treatment. The experimental errors were obtained by repeating the plasma modification procedure at least three times. The largest errors are observed for 5% O_2/He and Ar plasmas, where the concentration of oxidizing species in the plasma is low or not present at all. The higher the pressure, the weaker the oxidizing potential of plasma, which in the case of 5% O_2/He plasma results in wide distribution of measured values for higher total pressures in the plasma chamber. The low repeatability of results could stem from the higher reliance on primary post-plasma oxidation in air and thus lower control over the surface modification. Other contributions to the observed errors could originate from plasma inhomogeneity or from the dependence of post-plasma reactions in water on time elapsed from the end of plasma treatment.

The results of water contact angle measurements and calculated SFE allow following the changes induced by plasma immediately after the treatment as well as after sample immersion in water. The water contact angle (θ_w) for the reference sample is 96° ± 1.9 with a total SFE of 37.4 mJ/m^2 with a minimal polar component contribution (0.3 mJ/m^2). After the water immersion, the surface of the reference sample becomes

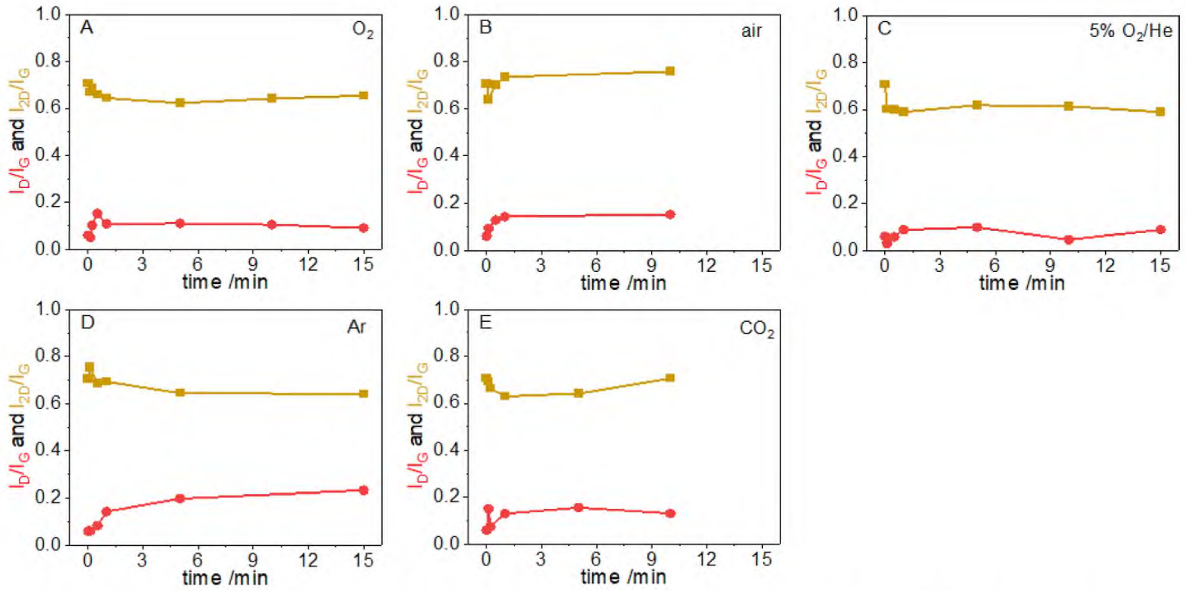

Fig. 5. Analysis of I_D/I_G and I_{2D}/I_G from Raman spectra of plasma-treated graphene paper samples. Time series are used for 0.2 mbar total pressure with gases A) 100% O_2, B) air; C) 5% O_2; D) Ar, and E) CO_2. (A colour version of this figure can be viewed online).

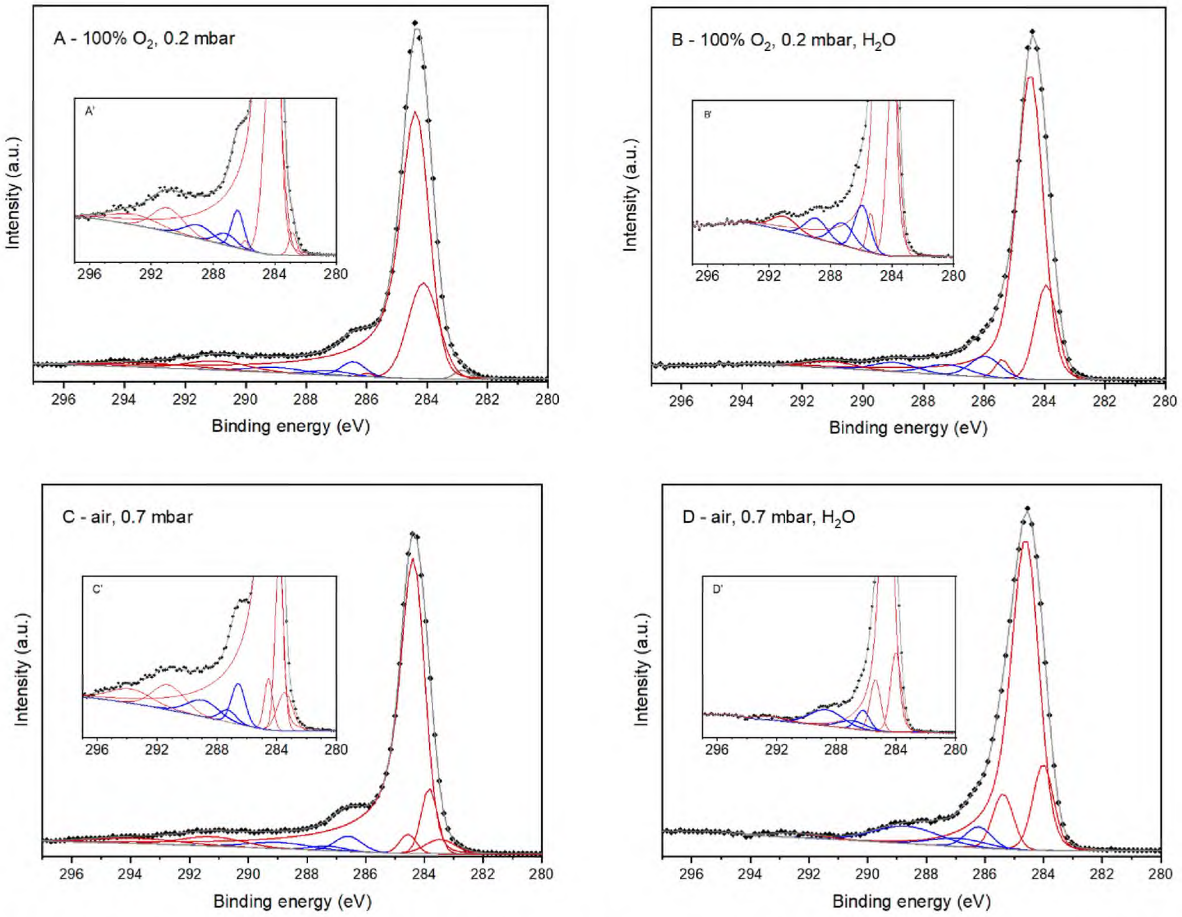

Fig. 6. XPS C 1s spectra and deconvolution of A) 100% O_2 plasma at 0.2 mbar total pressure – just after plasma, B) 100% O_2 plasma at 0.2 mbar total pressure – after water immersion, C) air plasma at 0.7 mbar total pressure – just after plasma, D) air plasma at 0.7 mbar total pressure – after water immersion. (A colour version of this figure can be viewed online).

more wettable ($\theta_w = 80.1° \pm 2.3$) with a slightly higher polar component of 4 mJ/m^2 (total SFE = 40.9 mJ/m^2). The effect of plasma treatment on θ_w and SFE for the investigated samples are presented in SI (Fig. S 4). In Fig. 3A the representative results for plasma-treated sample (parameters in Table S 1), for which the changes were most pronounced are presented. After exposure to plasma, graphene paper surface becomes hydrophilic with $\theta_w = 23.4° \pm 2.5$ immediately after the treatment, after immersion in water the surface preserves its hydrophilic properties, although θ_w increases to $34.3° \pm 2.2$. Plasma treatment has also a significant effect on total SFE which raises to 64.2 mJ/m^2 and 48.9 mJ/m^2 for the sample measured immediately after the treatment and after water immersion, respectively. The polar contribution of SFE differs significantly when compared calculations for both types of plasma-treated samples, i.e. immediately after the plasma treatment the polar component is 30.7 mJ/m^2 and decreases to 15.1 mJ/m^2 after water immersion. The design of experiment analysis based on water contact angle and SFE confirms the importance of exposure time optimization. However, the total pressure in plasma emerges here as an important contribution (Fig. 3B and C), similarly to 5% O_2/He with the work function changes as the response variable (Fig. S 3C).

To verify the structural integrity of the plasma-modified samples spectroscopic Raman characterization was performed. The Raman spectra for graphene paper samples treated with plasma in O_2, 5%O_2/He, air, CO_2, and Ar gases are presented in Fig. 4. Each of five individual spectra sets (A – E) compares the spectra of non-modified reference and samples treated with plasma using gradually increasing exposure time. For all samples, two intense characteristic G and 2D bands are present, located at ~1580 and ~2725 cm^{-1}, respectively. The G band is associated with the vibrational mode of graphitic carbon (E_{2g} optical mode) while the 2D band (also called G') is related to the two-phonon lattice vibrational process. The latter is divided into two components, which is typical for multilayer graphite materials as well as for bulk graphite [32].

Regardless of the gas used, no significant changes in Raman spectra upon plasma modification are observed. Only, a very low-intensity peak at ~1358 cm^{-1} appears, indicating that the plasma treatment is activating the disorder-induced D band. This band is due to the A_{1g} breathing modes of six-atom rings [33]. However, the very low intensities of appearing D bands indicate their low concentration and therefore the negligible extent of the plasma influence on the bulk structure of studied graphene paper. Moreover, the D' band at 1600 cm^{-1}, which is the next step of the carbon amorphization process does not appear at all. In turn, to analyze the effect of modification time the ratio of peak intensities I_D/I_G and I_{2D}/I_G were calculated and presented in Fig. 5. For each of the gases employed during plasma treatment, the values of the I_D/I_G ratio are practically constant, indicating no significant influence on the bulk structure of graphene paper, regardless of the exposure time.

The selected samples from the optimization series for each plasma type with the highest change in their work function (Fig. 3) were investigated with the use of the XPS. To determine the origin of the effect of water on the work function changes, the samples were transferred to the XPS vacuum chamber as soon as possible after plasma treatment and after water immersion. The comparison of C 1s spectra for 100% O_2 and air plasmas just after plasma treatment and after water immersion is presented in Fig. 6. Also, the spectra for the sample treated with 100%

Table 2
XPS-derived total surface oxygen content and relative oxygen functional groups content for plasma modified graphene paper samples.

Sample name/ plasma treatment	Total O	Total N	C 1s components			$\Delta\Phi$ (H2O)/ eV
			C–O/ C_{tot} [a]	C=O/ C_{tot}	COO/ C_{tot}	
Reference	2.2%	0%	2.2%	–	–	–
Reference + H_2O [b]	2.1%	0.2%	2.2%	–	–	–
100% O_2	6.8%	0%	2.2%	1.2%	1.9%	–
100% O_2 + H_2O	12.7%	0.5%	4.5%	3.2%	2.8%	0.46
Air	8.2%	0%	2.8%	1.0%	2.7%	–
Air + H_2O	20.9%	1.1%	3.5%	2.9%	7.3%	0.45
5% O_2/He	9.8%	0%	2.8%	3.0%	2.3%	–
5% O_2/He + H_2O	14.1%	1.3%	3.4%	3.1%	4.5%	0.26
CO_2	13.9%	0%	5.3%	2.4%	3.3%	–
CO_2 + H_2O	16.1%	0.7%	7.6%	5.2%	2.2%	0.32
Ar	6.7%	0%	2.2%	2.0%	1.4%	–
Ar + H_2O	11.6%	0.5%	4.6%	1.8%	2.9%	0.26

[a] C_{tot} – total area of C 1s peak; C–O, C=O, COO – area of individual components.
[b] Reference sample immersed in water and dried, according to the procedure for plasma-treated samples.

O_2 plasma at 0.7 mbar and 5 min were recorded and presented along with the reference graphene paper spectra in Fig. S 5. The C 1s range after 5% O_2/He, Ar and CO_2 plasmas are presented in Fig. S 6. The respective O 1s and N 1s XPS spectral ranges are shown in Fig. S 7 (reference, 100% O_2, air) and Fig. S 8 (5% O_2/He, CO_2, Ar).

The quantification of the surface composition based on the C 1s, O 1s, and N 1s spectral ranges is presented in Table 2. Total oxygen content, in the form of oxygen functional groups, increases substantially for all plasma-treated samples, regardless of the plasma type. A striking effect is observed for the water-immersed samples, for which the oxygen content increases even more. This effect is most pronounced for the air plasma and the least pronounced for the CO_2 plasma. However, while the air plasma-treated sample contains also the highest number of oxygen groups, the CO_2 plasma-treated sample is the second-highest in that respect. Interestingly, the speciation of the OFGs is entirely different for these plasma and water-treated samples, wherein for the air plasma the –COO type groups dominate and for CO_2 plasma it is the -C-O type groups. To verify the effect of total pressure in the plasma chamber on the number of surface oxygen groups we quantified the oxygen content in the sample treated with 100% O_2 plasma at 0.7 mbar (XPS spectra in Fig. S 5B and Fig. S 7C, D), for the modification time of maximum WF increase (5 min, $\Delta WF = 0.34$ eV, Fig. 2). After water immersion, the oxygen content was found to be 8.8 at.%, the lowest of all of the optimised samples for each plasma gas.

4. Discussion

The work function increase just after plasma treatment is caused by a combination of several possible effects. They include the insertion of surface functional groups in oxidative plasmas, surface oxidation in the air of the plasma-activated surface, creation of plasma-induced defects and disorder in carbon lattice as well as static electrification of the carbon material in plasma. Plasma oxidation combined with post-plasma reactions in the air is most pronounced for the 100% O_2 plasma gas at low pressure, where the maximum WF changes are obtained within seconds of plasma treatment. For weaker oxidative conditions, the time needed to reach maximum work function modification is longer, but the number of introduced oxygen groups can be similar. Plasma treatment does not deteriorate the structure of the material since the I_D/I_G ratio from the Raman spectra does not show any appreciable increase in the structural disorder. Immersion in water leads to further post-plasma reactions, which lead to a decrease in the work function and, surprisingly, to an increase in the number of oxygen functional groups. At the same time, the interaction with water results in a decrease in the surface free energy, very likely through the saturation of surface defects, i.e. dangling bonds, by creating oxygen functional groups.

4.1. Tuning the work function

The application of the design of experiments approach allowed to select the key parameter to optimize for maximum work function changes of the studied graphene paper material with different plasmas. Except for the 5% O_2/He plasma, the plasma treatment time was found to influence the most electronic properties of the materials. Very high initial $\Delta\Phi$, obtained just after plasma treatment was confirmed to decrease in time. The time scale of the changes is of the order of days (Fig. 1A) and may include mechanisms such as reactive desorption of surface oxygen groups by interaction with water vapour or oxygen [7]. We have noticed, however, that the samples are electrostatically charged after plasma, and such charging may substantially influence the V_{CPD} reading from the Kelvin probe [34,35]. Nevertheless, the graphene paper should quickly release the excessive change in contact with the metal holder during WF measurements, which is not observed – the initial short time scale changes are in the order of hours. It may be so due to the limited conductivity of graphene perpendicular to the hexagonal axis. The additional effect which may result in the WF decrease over a longer than anticipated period could be reciprocal stabilization of the extra charge and surface oxygen functional groups. From the practical point of view (sample shelf life, application in an aqueous conditions), the work function changes after immersion in water and drying can be more relevant (Fig. 1B). Except for the 100% O_2 plasma at 0.2 mbar, the values of $V_{CPD(asap)}$ and $V_{CPD(H2O)}$ exhibit a linear correlation (Fig. S 9), where final $V_{CPD(H2O)}$ values are higher than initial V_{CPD}. It indicates that the decisive changes to the graphene paper surface are induced during the plasma treatment and subsequent exposure to the air. The following water immersion stabilizes the activated, reactive surface and the changes are proportional to the initial plasma activation. Moreover, the estimated slopes of the linear function, which could be fitted to the $V_{CPD(H2O)}$ vs $V_{CPD(asap)}$ data in Fig. S 9 exhibit different slopes and intercepts, indicating plasma-specific effects.

Following the DoE analysis, it can be concluded that work function tuning can be achieved with better precision for 0.7 mbar total pressure of air in the chamber, rather than for 0.2 mbar total pressure of pure oxygen. The higher pressure of feeding gas in the plasma chamber results in milder conditions and thus slower surface activation and functionalization. It is reflected in the longer times required to reach the maximum of the work function for each material. In contrast, for 0.2 mbar total pressure of O_2, the initial changes, below 1 min, exhibit a complicated character. In summary, the application of the air plasma at 0.7 mbar total pressure allows for the highest range of work function increase with the controlled kinetics – the smoothest course of the $V_{CPD(H2O)}$ vs *time* curve. Lower reactive oxygen concentration, resulting from lower oxygen partial pressure or fragmentation of CO_2 does not allow for such high WF changes. The Ar plasma, which relies solely on the post plasma reactions in air and water allows the lowest range of the work function changes.

4.2. Surface functionalization

The surface composition of WF-optimised samples was investigated with the XPS, to determine whether the total surface oxygen concentration changes after immersion in water and to evaluate the speciation of oxygen functionalities. Based on Table 2, a distribution of oxygen among the three generic oxygen surface groups can be analysed. Using the simplest model [27], one has -C-O groups (hydroxyl), –C=O groups (carbonyl), where the area of the respective C 1s peak relative to total C 1s range signal represents both to the concentration of these groups and the concentration of oxygen bound within them. The third type of

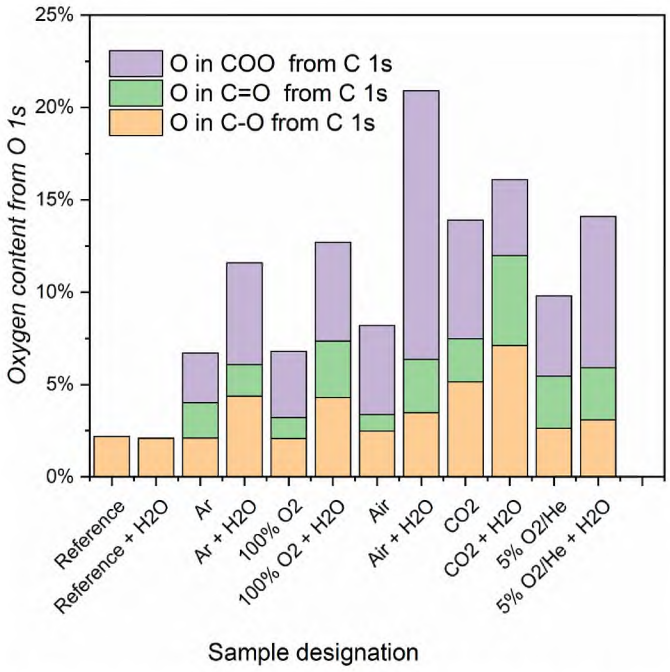

Fig. 7. Speciation analysis based on Table 2 and a simple model for oxygen functional groups. PL – plasma. (A colour version of this figure can be viewed online0.)

species is –COO groups (carboxyl), where the relative concentration of oxygen bound to carboxyl groups is two times higher than the concentration of these groups determined from their C 1s component, as presented in Fig. 7.

Interestingly, the same WF changes are observed for air and 100% O_2 plasma-treated samples, but the oxygen surface concentration is almost two times higher for the former (20.9 vs 12.7 at.%). On the other hand, similar oxygen surface concentrations for Ar and 100% O_2 yield very distinct $\Delta\Phi$ values (0.26 and 0.46 eV, respectively). Moreover, WF-optimised 5% O_2/He plasma treatment with subsequent water immersion allowed for the introduction of more surface oxygen groups (14.1 at.%) than 100% oxygen plasma (12.7 at.%), but the work function changes are significantly higher for the latter (0.26 vs 0.46 eV, Table 2). This analysis, limited to the samples for which the work function changes were maximized, shows that not only the number of surface oxygen groups but also their specification determines the surface electronic properties, such as WF. The air plasma-treated sample immersed in water contains the highest number of oxygen functional groups, but among them the fraction of the –COO type is the largest. It is different for 100% O_2 plasma, where the highest number of carbon atoms bonded to oxygen groups is in the form of -C-O type (see also Table 2). For Ar and 5% O_2 plasma-treated samples immersed in water the WF changes are similar, but the 5% O_2 treated sample has more surface oxygen, with a higher fraction of –COO groups. This rough qualitative analysis allows concluding that the –COO type groups contribute to a much lower extent to the work function changes by forming weaker surface dipoles than the -C-O type groups (hydroxyl groups). This observation can be corroborated by a recent work where similar conclusions were drawn [20].

The CO_2 plasma was used to study the possible enhanced formation of –COO type groups as observed for polymeric surfaces [36]. Interestingly, this plasma type allowed for the introduction of the highest number of oxygen functional groups, as measured just after plasma, with the highest fraction of –COO component. The surface stability of such a surface is also the highest, which is evidenced by the lowest oxygen content increase after immersion in water. The water stabilized sample can be tuned to intermediate maximum work function changes, with a decrease of the relative –COO type surface groups upon immersion in water. Interestingly, for this sample, the surface coverage with -C-O type groups is the highest, which is not reflected in the WF change of the surface. A tentative explanation is that these groups are formed on the additional carbon atoms inserted onto the surface, and form a different type of dipole than hydroxyl groups located directly on the surface defect sites.

5. Post-plasma reactivity in water

Based on the literature data, we hypothesized that the reactivity in the water of the plasma-treated graphene paper surface is due to the radicals present even after exposition to the air upon completion of the plasma treatment [22]. Therefore, we measured the EPR spectra of the GP just after plasma treatment and then after water immersion. We found that there are radicals present in the graphene paper, even for the unmodified materials. However, the plasma treatment results in an increase of the concentration of the radicals to c.a. 110% with respect to the untreated sample, while water immersion causes a decrease down to ~60%. It has to be noted, that the analysed graphene paper easily undergoes electrostatic charging, which influences the EPR measurement. The EPR spectra exhibited Dysonian lineshape, which is typical for conducting materials [37,38]. The determined g factor equal to 2.004 is usually observed for free radicals in carbon materials [39]. The hypothesis that the reactivity of graphene paper in water is due to the radicals was further verified. First, we checked if the radicals are formed upon UV irradiation of graphene paper. To that end, a graphene paper sample was subjected to UV irradiation *in situ* during the EPR measurement, and the results show that radicals were readily formed, but disappeared upon switching off the light source, Fig. 8A. The maximum increase in the concentration of the radicals was 25% (curve: 7 min), and this value stabilized within several minutes after turning on the light source. To evidence the role of radicals on the electronic properties of graphene paper we also performed *in situ* work function measurement, where UV light (260 nm) was shone on the surface of GP. The work function gradually increased after turning the light source on, and similarly gradually decreased after turning it off, Fig. 8B. These observations may explain why a gradual decrease in WF values is observed after removing the sample from the plasma chamber. Plasma treatment

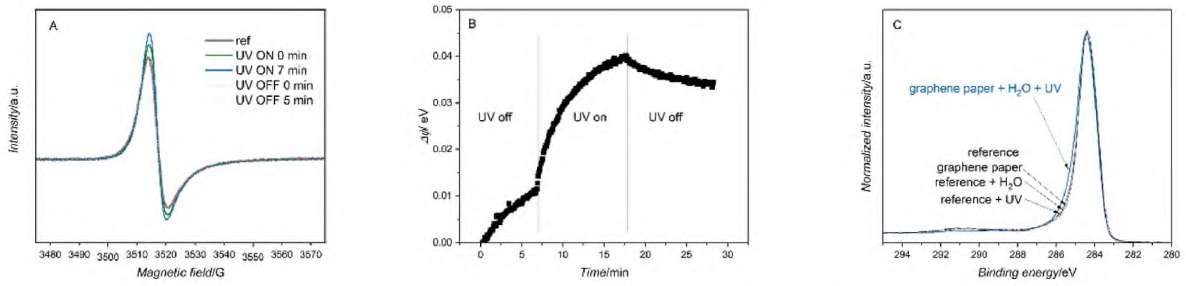

Fig. 8. A) EPR spectra changes of the spectrum upon UV irradiation; B) WF changes upon UV irradiation, C) XPS O 1s, N 1s and C 1s spectra of UV treated sample before and after water immersion. (A colour version of this figure can be viewed online).

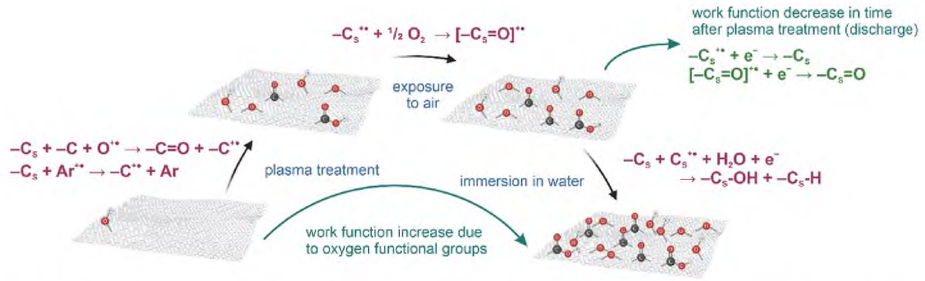

Fig. 9. A simplified scheme of plasma and post-plasma modification of graphene paper surface. $–C_S$ denotes a fragment of the graphene surface rather than a single carbon atom. Only the simplest forms of oxygen functional groups are included in the chemical reactions. (A colour version of this figure can be viewed online).

results in the formation of both stable and unstable radicals, and in a short time scale a deexcitation of the unstable radical species occurs leading to a relatively fast work function decrease. Furthermore, to obtain the final piece of evidence of the surface radicals' reactivity we subjected the GP sample to UV irradiation for 15 min and then immersed it in water, as in the procedure for plasma-treated samples. We investigated the sample by XPS and found an increase in oxygen surface concentration from 2.2% to 5%, while the UV light alone, without water immersion, did not affect the surface composition, Fig. 8C. Similarly, immersion in water alone did not increase the OFG concentration, Table 2. The changes in the work function and carrier concentration upon ultraviolet irradiation have been previously reported, and it was shown that ultraviolet irradiation may lead to oxygen desorption, thus reducing the hole density and work function of graphene [40]. In our case, however, the work function changes, are one order of magnitude smaller in comparison with plasma functionalization, indicating minute changes in the surface coverage. Observed changes can be attributed to the additional functionalization of graphene with oxygen in very small surface concentrations, not detectable in the XPS spectra [41].

The effect of different plasma types on the post-plasma reactivity in water can be rationalized based on the plasma gas emission spectra in the plasma chamber. The emission spectra of different plasmas are collected in Fig. S10. The measurements were taken through the quartz window of the plasma chamber, and the results are comparable to the spectra reported in the literature [42–44]. It was reported that carbon structures of graphene or nanotubes may undergo photooxidation in water under UV light irradiation [41,45,46]. For the plasma gasses applied, the strongest post-plasma reaction in water is observed for the air plasma, for which the nitrogen present in the chamber results in high light emission between 300 and 400 nm. The delayed effect of oxidation during water immersion can be explained by the stabilization of free radicals in the graphene resonance rings, whereas the radicals are created by plasma irradiation [22]. Interestingly, CO_2 plasma also emits radiation below 400 nm. In this case, however, we hypothesise that the grafting of carbon atoms on the graphenic surface leads to a decreased stabilization of radicals. Less stable radicals would exhibit an increased reactivity in air and a more stable resulting surface i.e. less reactive in water, which is what we observe for this sample.

6. Conclusions

A complementary optimization of graphene paper surface plasma modification with five different gases is presented in terms of work function optimization. To stabilize the carbon materials after plasma exposure, the samples were immersed in water. Based on our observations we propose a simplified scheme, where subsequent functionalization of the graphene paper takes place, Fig. 9. Primary reactions of plasma-activated surface occur during the sample exposure to the air, as confirmed by the Ar plasma treatment. However, the surface of graphene paper after the post-plasma reactions in the air is still highly reactive, as demonstrated by the work function changes measurements. Immersion in water results in a stable surface of graphene paper exemplified in the constant values of the work function. At the same time, the oxygen functional group concentration increases in comparison with plasma-treated-only samples.

We showed that the concentration of carbon radicals increases after plasma treatment and disappears after immersion in water. At the same time, UV irradiation of graphene paper brings about an increase in carbon radicals concentration which coincides with a work function increase. Moreover, we observed an increase in the surface oxygen functional group concentration in the non-plasma UV irradiated sample immersed in water. Therefore, we concluded that the increase of the surface oxygen group concentration after plasma treatment and subsequent immersion in water results from secondary post-plasma reactions involving radicals. This implies that the most pronounced effects of the plasma treatment on the work function changes, without water immersion, are due to electrostatic charging and radical formation under plasma irradiation.

From a practical standpoint, one has to be careful to study a stable surface not exhibiting the post-plasma reactivity or electrostatic charging to fine-tune the work function of the graphene paper and related materials. Finally, for a controlled work function modification, it is most beneficial to use mild plasma conditions by applying high total pressure and decreased oxygen partial pressure. The application of different plasma gasses can be used to additionally tune oxygen content and its speciation for the desired work function changes.

CRediT authorship contribution statement

Paweł Stelmachowski: Conceptualization, Methodology, Formal analysis, (XPS), Resources, Writing – original draft, Writing – review & editing, Supervision, Project administration, Funding acquisition. **Karolina Kadela:** Investigation, (Plasma modification, WF, Raman, CA), Formal analysis, (WF, CA), Data curation. **Gabriela Grzybek:** Formal analysis, (Raman), Writing – original draft, Writing – review & editing, Supervision. **Monika Gołda-Cępa:** Methodology, (CA), Writing – review & editing, Supervision. **Krzysztof Kruczała:** Investigation, (EPR), Formal analysis, (EPR), Writing – review & editing. **Andrzej Kotarba:** Conceptualization, Writing – review & editing.

Declaration of competing interest

The authors declare that they have no known competing financial interests or personal relationships that could have appeared to influence the work reported in this paper.

Acknowledgements/Funding

This study was financially supported by the National Science Centre, Poland, project number 2020/37/B/ST5/01876.

Appendix A. Supplementary data

Supplementary data to this article can be found online at https://doi.

org/10.1016/j.carbon.2022.07.031.

References

[1] P. Legutko, W. Kaspera, T. Jakubek, P. Stelmachowski, A. Kotarba, Influence of potassium and NO addition on catalytic activity in soot combustion and surface properties of iron and manganese spinels, Top. Catal. (2013) 745–749, https://doi.org/10.1007/s11244-013-0026-1.

[2] P. Stelmachowski, K. Ciura, G. Grzybek, Morphology-dependent reactivity of cobalt oxide nanoparticles in N2O decomposition, Catal. Sci. Technol. 6 (2016) 5554–5560, https://doi.org/10.1039/c6cy00365f.

[3] A. Davó-Quiñonero, I. Such-Basáñez, J. Juan-Juan, D. Lozano-Castelló, P. Stelmachowski, G. Grzybek, A. Kotarba, A. Bueno-López, New insights into the role of active copper species in CuO/Cryptomelane catalysts for the CO-PROX reaction, Appl. Catal. B Environ. 267 (2020), 118372, https://doi.org/10.1016/j.apcatb.2019.118372.

[4] S. Wójcik, G. Grzybek, P. Stelmachowski, Z. Sojka, A. Kotarba, Bulk, surface and interface promotion of Co3O4 for the low-temperature N2O decomposition catalysis, Catalysts 10 (2020) 1–12, https://doi.org/10.3390/catal10010041.

[5] S. Naghdi, G. Sanchez-Arriaga, K.Y. Rhee, Tuning the work function of graphene toward application as anode and cathode, J. Alloys Compd. 805 (2019) 1117–1134, https://doi.org/10.1016/j.jallcom.2019.07.187.

[6] J. Duch, P. Stelmachowski, A.H.A. Monteverde Videla, M. Gajewska, A. Kotarba, S. Specchia, Thermal oxygen activation followed by in situ work function measurements over carbon-supported noble metal-based catalysts, Int. J. Hydrogen Energy 44 (2019) 16648–16656, https://doi.org/10.1016/j.ijhydene.2019.04.130.

[7] J. Duch, M. Gołda-Cępa, W. Piskorz, J. Rysz, A. Kotarba, Stability of oxygen-functionalized graphenic surfaces: theoretical and experimental insights into electronic properties and wettability, Appl. Surf. Sci. 539 (2021), 148190, https://doi.org/10.1016/j.apsusc.2020.148190.

[8] W. Pajerski, J. Duch, D. Ochonska, M. Golda-Cepa, M. Brzychczy-Wloch, A. Kotarba, Bacterial attachment to oxygen-functionalized graphenic surfaces, Mater. Sci. Eng. C. 113 (2020), 110972, https://doi.org/10.1016/j.msec.2020.110972.

[9] J. Duch, M. Golda-Cepa, A. Kotarba, Evaluating the effect of oxygen groups attached to the surface of graphenic sheets on bacteria adhesion: the role of the electronic factor, Appl. Surf. Sci. 463 (2019) 1134–1140, https://doi.org/10.1016/j.apsusc.2018.08.237.

[10] G.A. Somorjai, Y. Li, Introduction to Surface Chemistry and Catalysis, second ed., Wiley, New York, 2010.

[11] S. Datta, P. Singh, D. Jana, C.B. Chaudhuri, M.K. Harbola, D.D. Johnson, A. Mookerjee, Exploring the role of electronic structure on photo-catalytic behavior of carbon-nitride polymorphs, Carbon N. Y. 168 (2020) 125–134, https://doi.org/10.1016/j.carbon.2020.04.008.

[12] J. Duch, M. Mazur, M. Golda-Cepa, J. Podobiński, W. Piskorz, A. Kotarba, Insight into modification of electrodonor properties of multiwalled carbon nanotubes via oxygen plasma: surface functionalization versus amorphization, Carbon N. Y. 137 (2018) 425–432, https://doi.org/10.1016/j.carbon.2018.05.059.

[13] C.H. Lin, M.S. Tsai, W.T. Chen, Y.Z. Hong, P.Y. Chien, C.H. Huang, W.Y. Woon, C. T. Lin, A low-damage plasma surface modification method of stacked graphene bilayers for configurable wettability and electrical properties, Nanotechnology 30 (2019), https://doi.org/10.1088/1361-6528/ab0511.

[14] J.J. Zeng, Y.J. Lin, Tuning the work function of graphene by nitrogen plasma treatment with different radio-frequency powers, Appl. Phys. Lett. 104 (2014), 233103, https://doi.org/10.1063/1.4882159.

[15] A. Benko, D. Medina-Cruz, J. Duch, T. Popiela, S. Wilk, M. Bińczak, M. Nocuń, E. Menaszek, L.D. Geoffrion, G. Guisbiers, A. Kotarba, T.J. Webster, Conductive all-carbon nanotube layers: results on attractive physicochemical, anti-bacterial, anticancer and biocompatibility properties, Mater. Sci. Eng. C. 120 (2021), 111703, https://doi.org/10.1016/j.msec.2020.111703.

[16] J.Y. Cheon, J.H. Kim, J.H. Kim, K.C. Goddeti, J.Y. Park, S.H. Joo, Intrinsic relationship between enhanced oxygen reduction reaction activity and nanoscale work function of doped carbons, J. Am. Chem. Soc. 136 (2014) 8875–8878, https://doi.org/10.1021/ja503557x.

[17] M. Sharma, J.H. Jang, D.Y. Shin, J.A. Kwon, D.H. Lim, D. Choi, H. Sung, J. Jang, S. Y. Lee, K.Y. Lee, H.Y. Park, N. Jung, S.J. Yoo, Work function-tailored graphene via transition metal encapsulation as a highly active and durable catalyst for the oxygen reduction reaction, Energy Environ. Sci. 12 (2019) 2200–2211, https://doi.org/10.1039/c9ee00381a.

[18] H. Ago, Work functions and surface functional groups of multiwall carbon nanotubes, J. Phys. Chem. B 103 (1999) 8116–8121, https://doi.org/10.1021/jp991659y.

[19] N. Hordy, J.L. Meunier, S. Coulombe, Thermal stability of plasma generated oxygenated functionalities on carbon nanotubes, Plasma Process. Polym. 12 (2015) 533–544, https://doi.org/10.1002/ppap.201400195.

[20] J.S.D. Rodriguez, T. Ohigashi, C.C. Lee, M.H. Tsai, C.C. Yang, C.H. Wang, C. Chen, W.F. Pong, H.C. Chiu, C.H. Chuang, Modulating chemical composition and work function of suspended reduced graphene oxide membranes through electrochemical reduction, Carbon N. Y. 185 (2021) 410–418, https://doi.org/10.1016/j.carbon.2021.09.015.

[21] A. Kostuch, S. Jarczewski, M.K. Surówka, P. Kuśtrowski, Z. Sojka, K. Kruczała, The joint effect of electrical conductivity and surface oxygen functionalities of carbon supports on the oxygen reduction reaction studied over bare supports and Mn–Co spinel/carbon catalysts in alkaline media, Catal. Sci. Technol. 11 (2021) 7578–7591, https://doi.org/10.1039/D1CY01115D.

[22] F. Khelifa, S. Ershov, Y. Habibi, R. Snyders, P. Dubois, Free-radical-induced grafting from plasma polymer surfaces, Chem. Rev. 116 (2016) 3975–4005, https://doi.org/10.1021/acs.chemrev.5b00634.

[23] A. Merenda, E. Des Ligneris, K. Sears, T. Chaffraix, K. Magniez, D. Cornu, J. A. Schütz, L.F. Dumée, Assessing the temporal stability of surface functional groups introduced by plasma treatments on the outer shells of carbon nanotubes, Sci. Rep. 6 (2016), https://doi.org/10.1038/srep31565.

[24] J.I. Mendez-Linan, E. Ortiz-Ortega, M.F. Jimenez-Moreno, M.I. Mendivil-Palma, E. Martínez-Guerra, F.S. Aguirre-Tostado, S.O. Martinez-Chapa, S. Hosseini, M. J. Madou, Aging effect of plasma-treated carbon surfaces: an overlooked phenomenon, Carbon N. Y. 169 (2020) 32–44, https://doi.org/10.1016/j.carbon.2020.06.085.

[25] E. Ortiz-Ortega, S. Hosseini, S.O. Martinez-Chapa, M.J. Madou, Aging of plasma-activated carbon surfaces: challenges and opportunities, Appl. Surf. Sci. 565 (2021), https://doi.org/10.1016/j.apsusc.2021.150362.

[26] N. Fairley, V. Fernandez, M. Richard-Plouet, C. Guillot-Deudon, J. Walton, E. Smith, D. Flahaut, M. Greiner, M. Biesinger, S. Tougaard, D. Morgan, J. Baltrusaitis, Systematic and collaborative approach to problem solving using X-ray photoelectron spectroscopy, Appl. Surf. Sci. Adv. 5 (2021), https://doi.org/10.1016/j.apsadv.2021.100112.

[27] M. Smith, L. Scudiero, J. Espinal, J.S. McEwen, M. Garcia-Perez, Improving the deconvolution and interpretation of XPS spectra from chars by ab initio calculations, Carbon N. Y. 110 (2016) 155–171, https://doi.org/10.1016/j.carbon.2016.09.012.

[28] R. Blume, D. Rosenthal, J.P. Tessonnier, H. Li, A. Knop-Gericke, R. Schlögl, Characterizing graphitic carbon with X-ray photoelectron spectroscopy: a step-by-step approach, ChemCatChem 7 (2015) 2871–2881, https://doi.org/10.1002/cctc.201500344.

[29] A. Badr, General introduction to design of experiments (DOE), in: I. Akyar (Ed.), Wide Spectra Qual. Control, InTech, 2011, https://doi.org/10.5772/23878.

[30] B. Durakovic, Design of experiments application, concepts, examples: state of the art, Period. Eng. Nat. Sci. 5 (2017) 421–439, https://doi.org/10.21533/pen.v5i3.145.

[31] A. Grandoni, G. Mannini, A. Glisenti, A. Manariti, G. Galli, Use of statistical design of experiments for surface modification of Kapton films by CF 4 O 2 microwave plasma treatment, Appl. Surf. Sci. 420 (2017) 579–585, https://doi.org/10.1016/j.apsusc.2017.05.140.

[32] A.C. Ferrari, J.C. Meyer, V. Scardaci, C. Casiraghi, M. Lazzeri, F. Mauri, S. Piscanec, D. Jiang, K.S. Novoselov, S. Roth, A.K. Geim, Raman spectrum of graphene and graphene layers, Phys. Rev. Lett. 97 (2006) 1–4, https://doi.org/10.1103/PhysRevLett.97.187401.

[33] A.C. Ferrari, D.M. Basko, Raman spectroscopy as a versatile tool for studying the properties of graphene, Nat. Nanotechnol. 8 (2013) 235–246, https://doi.org/10.1038/nnano.2013.46.

[34] J. Yin, B. Vanderheyden, B. Nysten, Dynamic charge transfer between polyester and conductive fibres by Kelvin probe force microscopy, J. Electrost. 96 (2018) 30–39, https://doi.org/10.1016/j.elstat.2018.09.006.

[35] J. Yin, B. Nysten, Contact electrification and charge decay on polyester fibres: a KPFM study, J. Electrost. 96 (2018) 16–22, https://doi.org/10.1016/j.elstat.2018.09.002.

[36] L. Lin, L. Rui, C. Li, Q. Liu, S. Li, Y. Xia, H. Hu, W. Yang, H. Xu, Study on CO2-based plasmas for surface modification of polytetrafluoroethylene and the wettability effects, J. CO2 Util. 53 (2021), https://doi.org/10.1016/j.jcou.2021.101752.

[37] G. Feher, A.F. Kip, Electron spin resonance absorption in metals. I. Experimental, Phys. Rev. 98 (1955) 337–348, https://doi.org/10.1103/PhysRev.98.337.

[38] F.J. Dyson, Electron spin resonance absorption in metals. II. Theory of electron diffusion and the skin effect, Phys. Rev. 98 (1955) 349–359, https://doi.org/10.1103/PhysRev.98.349.

[39] Ł. Łańcucki, S. Schlick, M. Danilczuk, F.D. Coms, K. Kruczała, Sulfonated poly (benzoyl paraphenylene) as a membrane for PEMFC: ex situ and in situ experiments of thermal and chemical stability, Polym. Degrad. Stabil. 98 (2013) 3–11, https://doi.org/10.1016/j.polymdegradstab.2012.11.004.

[40] Y.J. Lin, J.J. Zeng, Tuning the work function of graphene by ultraviolet irradiation, Appl. Phys. Lett. 102 (2013), 183120, https://doi.org/10.1063/1.4804289.

[41] X. Cao, J. Zhao, Z. Wang, B. Xing, New insight into the photo-transformation mechanisms of graphene oxide under UV-A, UV-B and UV-C lights, J. Hazard Mater. 403 (2021), https://doi.org/10.1016/j.jhazmat.2020.123683.

[42] P. Attri, F. Tochikubo, J.H. Park, E.H. Choi, K. Koga, M. Shiratani, Impact of Gamma rays and DBD plasma treatments on wastewater treatment, Sci. Rep. 8 (2018) 1–11, https://doi.org/10.1038/s41598-018-21001-z.

[43] M.I. Khan, N.U. Rehman, S. Khan, N. Ullah, A. Masood, A. Ullah, Spectroscopic study of CO2 and CO2-N2 mixture plasma using dielectric barrier discharge, AIP Adv. 9 (2019), https://doi.org/10.1063/1.5096399.

[44] D. Ray, R. Saha, S. Ch, DBD plasma assisted CO2 decomposition: influence of diluent gases, Catalysts 7 (2017) 244, https://doi.org/10.3390/catal7090244.

[45] N.T. Alvarez, C. Kittrell, H.K. Schmidt, R.H. Hauge, P.S. Engel, J.M. Tour, Selective photochemical functionalization of surfactant-dispersed single wall carbon nanotubes in water, J. Am. Chem. Soc. 130 (2008) 14227–14233, https://doi.org/10.1021/ja804164y.

[46] F. Xhyliu, G. Ao, Surface coating- and light-controlled oxygen doping of carbon nanotubes, J. Phys. Chem. C 125 (2021) 9236–9243, https://doi.org/10.1021/acs.jpcc.1c00257.